ANTIOXIDANTS & REDOX SIGNALING
Volume 22, Number 10, 2015

DOI: 10.1089/ars.2014.6017

Discoveries

ORIGINAL RESEARCH COMMUNICATION

CNC-bZIP Protein Nrf1-Dependent Regulation of Glucose-Stimulated Insulin Secretion

Hongzhi Zheng,[1,2,*] Jingqi Fu,[2,3,*] Peng Xue,[2,4,*] Rui Zhao,[5] Jian Dong,[2,6] Dianxin Liu,[7] Masayuki Yamamoto,[8] Qingchun Tong,[9] Weiping Teng,[1] Weidong Qu,[4] Qiang Zhang,[2] Melvin E. Andersen,[2] and Jingbo Pi[2,3]

Abstract

Aims: The inability of pancreatic β-cells to secrete sufficient insulin in response to glucose stimulation is a major contributing factor to the development of type 2 diabetes (T2D). We investigated both the *in vitro* and *in vivo* effects of deficiency of nuclear factor-erythroid 2-related factor 1 (Nrf1) in β-cells on β-cell function and glucose homeostasis. ***Results:*** Silencing of *Nrf1* in β-cells leads to a pre-T2D phenotype with disrupted glucose metabolism and impaired insulin secretion. Specifically, MIN6 β-cells with stable knockdown of *Nrf1* (*Nrf1*-KD) and isolated islets from β-cell-specific *Nrf1*-knockout [*Nrf1*(b)-KO] mice displayed impaired glucose responsiveness, including elevated basal insulin release and decreased glucose-stimulated insulin secretion (GSIS). *Nrf1*(b)-KO mice exhibited severe fasting hyperinsulinemia, reduced GSIS, and glucose intolerance. Silencing of *Nrf1* in MIN6 cells resulted in oxidative stress and altered glucose metabolism, with increases in both glucose uptake and aerobic glycolysis, which is associated with the elevated basal insulin release and reduced glucose responsiveness. The elevated glycolysis and reduced glucose responsiveness due to *Nrf1* silencing likely result from altered expression of glucose metabolic enzymes, with induction of high-affinity hexokinase 1 and suppression of low-affinity glucokinase. ***Innovation:*** Our study demonstrated a novel role of Nrf1 in regulating glucose metabolism and insulin secretion in β-cells and characterized Nrf1 as a key transcription factor that regulates the coupling of glycolysis and mitochondrial metabolism and GSIS. ***Conclusion:*** Nrf1 plays critical roles in regulating glucose metabolism, mitochondrial function, and insulin secretion, suggesting that Nrf1 may be a novel target to improve the function of insulin-secreting β-cells. *Antioxid. Redox Signal.* 22, 819–831.

Introduction

DIABETES IS A METABOLIC DISORDER mediated by genetic and environmental factors with a progressive loss of functional pancreatic β-cells (2). Type 1 diabetes (T1D) is an autoimmune disease with an absolute deficiency of insulin-producing β-cells. In contrast, type 2 diabetes (T2D) is characterized by peripheral insulin resistance and relative insulin deficiency in the early stage, followed by β-cell toxicity in the late stage of the disease (2, 36). β-cells respond to glucose by both producing and secreting insulin (2). The inability of β-cells to secrete sufficient insulin in response to glucose stimulation is a major contributing factor to the development of T2D (36). Before the onset of clinical T2D, β-cells compensate for increased insulin resistance in peripheral tissues by hyper-secreting insulin (36). In some T2D patients, basal insulin levels may be elevated to approximately twice normal values (41). Eventually, β-cells fail to meet the increasing metabolic

[1]The First Affiliated Hospital, China Medical University, Shenyang, China.
[2]Institute for Chemical Safety Sciences, The Hamner Institutes for Health Sciences, Research Triangle Park, North Carolina.
[3]School of Public Health, China Medical University, Shenyang, China.
[4]School of Public Health, Fudan University, Shanghai, China.
[5]School of Forensic Medicine, China Medical University, Shenyang, China.
[6]Institute of Medicine and Biology, Wuhan University of Science and Technology, Wuhan, China.
[7]Metabolic Signaling and Disease Program, Sanford-Burnham Medical Research Institute, Orlando, Florida.
[8]Department of Medical Biochemistry, Tohoku University Graduate School of Medicine, Sendai, Japan.
[9]Center for Metabolic and Degenerative Disease, The University of Texas Health Sciences Center at Houston, Houston, Texas.
*These three authors contributed equally to this work.

Innovation

Impairment of pancreatic β-cell function, in particular reduced glucose-stimulated insulin secretion (GSIS), is a critical event in the pathophysiology of type 2 diabetes (T2D). We found that β-cell-specific silencing of nuclear factor-erythroid 2-related factor 1 (Nrf1) led to a β-cell phenotype reminiscent of the early stage of T2D with disrupted β-cell glucose metabolism, marked elevation of basal insulin release, reduced GSIS, fasting hyperinsulinemia, and glucose intolerance. The impaired glucose sensing and insulin secretion of Nrf1 deficient β-cells are associated with aberrant expression of a group of glucose metabolic enzymes, leading to altered glucose metabolism in the cells. Our study suggests that Nrf1 may be a novel target to improve β-cell function.

demand, loss of β-cells occurs, and the majority of T2D patients become insulin dependent (12). Therefore, impairment of pancreatic β-cell function, in particular reduced glucose-stimulated insulin secretion (GSIS), is a critical event in the pathophysiology of T2D (2, 12, 36, 41). Numerous mechanisms, including impaired mitochondrial metabolism, oxidative stress, inflammation, endoplasmic reticulum (ER) stress, apoptosis, and perturbations in the ubiquitin-proteasome system (UPS), may play roles in the impairment of GSIS and β-cell damage (3, 10–12, 14, 34, 35, 38). However, we do not understand the exact mode of β-cell failure in T2D.

Nuclear factor-erythroid 2-related factor 1 (Nrf1, also known as NFE2L1/LCRF1/TCF11) belongs to the CNC-bZIP family of transcription factors (TFs), which also includes Nrf2, a canonical TF mediating the antioxidant response (6). Nrf1 is ubiquitously expressed in a wide range of tissues and it serves as an important regulator of antioxidant response, proteasome homeostasis, mitochondrial respiration, apoptosis, inflammation, lipid metabolism, and cell differentiation (6, 19, 20, 37, 40). As with the human analog, the mouse *Nrf1* gene is transcribed in multiple alternatively spliced forms, resulting in at least six protein isoforms containing 313, 453, 572, 583, 741, and 742 amino acids (aa), respectively. In addition, post-translational modifications, including glycosylation and proteolytic processing, play important roles in the transactivation and stabilization of various isoforms of Nrf1 (47, 48). Global *Nrf1* knockout (KO), which deletes all isoforms of Nrf1, results in embryonic lethality at mid-gestation in mice (8). Neuron-specific deletion of all-isoform *Nrf1* results in oxidative stress, UPS dysfunction, and neurodegeneration (21, 25). Hepatocyte-specific all-isoform *Nrf1*-KO mice develop severe hepatic steatosis and liver carcinoma (19, 44). Conditional KO of *Nrf1* in the bone leads to reduced bone size in mice (20). These findings suggest that some, if not all, isoforms of Nrf1 play important physiological role(s) in a variety of cells. However, the expression and function of Nrf1 in pancreatic β-cells have not yet been reported.

In this study, we found that silencing of all isoforms of Nrf1 in MIN6 β-cells and mouse islets led to marked elevation of basal insulin release with reduced GSIS, a β-cell phenotype reminiscent of the early stage of T2D. The impaired glucose sensing and insulin secretion of *Nrf1* deficient β-cells are associated with altered glucose metabolism, oxidative stress, and impaired ATP production in the cells. Clearly, Nrf1 plays critical roles in regulating glucose metabolism, mitochondrial function, and insulin secretion.

Results

Stable silencing of Nrf1 impairs insulin secretion in MIN6 β-cells

To determine the function of Nrf1 in pancreatic β-cells, we developed a line of MIN6 β-cells with stable knockdown of nearly all isoforms of Nrf1 (termed as *Nrf1*-KD) by using an shRNA primarily against the isoform-313, −453, −572, −583, −741, and −742 (Supplementary Fig. S1; Supplementary Data are available online at www.liebertpub.com/ars). Compared with the MIN6 cells expressing nonspecific control shRNA (Scramble), *Nrf1*-KD cells have significantly reduced expression of *Nrf1* mRNA, as determined by real-time reverse transcription-quantitative PCR (RT-qPCR) with a primer set targeting a common sequence of all the six isoforms of *Nrf1* described earlier (Fig. 1A). Immunoblotting using an antibody (sc-13031X; H-285) against an epitope corresponding to amino acids 191–475, mapped near the N-terminus of human Nrf1 (Supplementary Fig. S2A), and an antibody (sc-721; C-19) against the C-terminus (Supplementary Fig. S2B) showed that multiple bands with apparent molecular weight (MW) approximately at 65–160 kDa were diminished by knockdown. Among them, the isoform with an apparent MW at about 65 kDa was highly expressed in Scramble cells and dramatically decreased in *Nrf1*-KD cells, suggesting that this protein is the major isoform of Nrf1 in MIN6 cells and is critical to β-cell function. In agreement with previous studies showing that Nrf1 regulates the transcription of a variety of antioxidant enzymes (33, 49), Nrf1 silencing resulted in decreased intracellular levels of reduced glutathione (GSH) and elevated reactive oxygen species (ROS) accumulation (Fig. 1B, C). The levels of oxidized glutathione (GSSG) in *Nrf1*-KD and Scramble MIN6 cells were too low to be measured using the method previously described (34).

Although deficiency of all isoforms of Nrf1 did not significantly affect the basal expression of insulin at the mRNA (Fig. 1D) or protein (Fig. 1E) level, *Nrf1*-KD MIN6 cells had higher basal insulin release, with lower GSIS (Fig. 1F). The ratio of insulin secretion under high glucose (20 m*M*) to that under basal condition (3 m*M* glucose) was 11.7 times lower in *Nrf1*-KD cells than that of Scramble cells. Nonetheless, the insulin release in response to 30 m*M* KCl was comparable between *Nrf1*-KD and Scramble-treated cells (Fig. 1F). In addition, *Nrf1*-KD MIN6 cells released much more insulin than Scramble cells did under 3 m*M* of fructose or 3 m*M* of mannose condition. In contrast, insulin secretion under 3 m*M* of galactose showed no significant difference between *Nrf1*-KD and Scramble MIN6 cells (Supplementary Fig. S3).

Pancreatic β-cell-specific Nrf1-knockout mice have severe hyperinsulinemia

To further study the role of Nrf1 in β-cell function, we generated a line of mice with specific deletion of *Nrf1* in pancreatic β-cells. Compared with wild-type littermates [*Nrf1*(b)-WT], the only tissue with reduced *Nrf1* mRNA in the β-cell-specific *Nrf1*-knockout [*Nrf1*(b)-KO] mice was the islets. No changes were seen in mRNA for this variant in heart, liver, skeletal muscle, or spleen (Supplementary Fig. S4). In the brain, the mRNA expression of *Nrf1* slightly

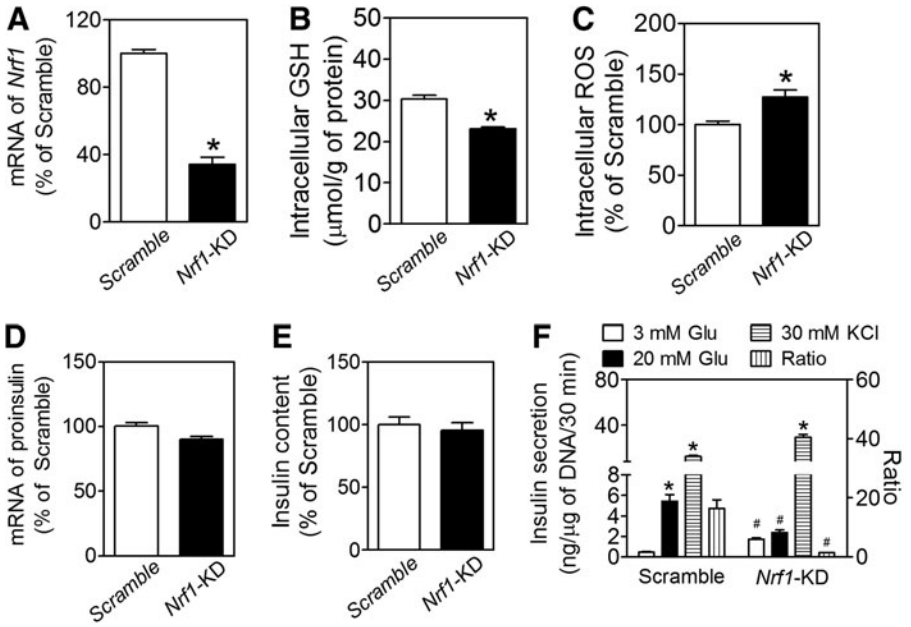

FIG. 1. Effects of *Nrf1* silencing on intracellular levels of GSH and ROS and insulin secretion in MIN6 β-cells. **(A)** mRNA expression of *Nrf1* determined by real-time RT-qPCR. The primer set detects isoform-313, −453, −572, −583, −741, and −742 of *Nrf1*. Scramble, cells transduced with nontarget negative control shRNA; *Nrf1*-KD, cells with knockdown of *Nrf1*. $n=9$–12. $^{*}p<0.05$ *versus* Scramble. **(B)** Intracellular levels of GSH. $n=9$. $^{*}p<0.05$ *versus* Scramble. **(C)** Intracellular ROS levels. $n=11$. $^{*}p<0.05$ *versus* Scramble. **(D)** mRNA expression of proinsulin. $n=6$–9. **(E)** Insulin content. $n=13$–36. **(F)** Insulin secretion. Glu, glucose; KCl, potassium chloride; ratio, insulin secreted under 20 m*M* over 3 m*M* Glu. $n=19$–21. $^{*}p<0.05$ *versus* the same cell types with 3 m*M* Glu; $^{\#}p<0.05$ *versus* Scramble with the same treatment. *Nrf1*, nuclear factor-erythroid 2-related factor 1; ROS, reactive oxygen species; RT-qPCR, reverse transcription-quantitative PCR.

decreased in the hypothalamus, but not in cerebrum and cerebellum, an observation consistent with the expression pattern of Cre combinase of RIP-Cre mice (43). On a normal chow diet, *Nrf1*(b)-KO mice had similar food intake to their littermates. However, both male and female *Nrf1*(b)-KO mice gained weight at a slightly higher rate (Supplementary Fig. S5A) and by week 13–17, they had a marginally higher average body weight than *Nrf1*(b)-WT mice (Supplementary Fig. S5B). Consistent with the changes in body weight, male *Nrf1*(b)-KO mice showed larger retroperitoneal and epididymal visceral white adipose tissue pads compared with their wild-type littermates (Supplementary Fig. S5C).

The deficiency of *Nrf1* in β-cells did not significantly affect fasting or nonfasting blood glucose levels (Fig. 2A). However, *Nrf1*(b)-KO mice, in particular males, developed severe hyperinsulinemia (Fig. 2B, C) with glucose intolerance (Supplementary Fig. S6). The average fasting plasma insulin level in male *Nrf1*(b)-KO mice was about 6.0 times higher than that of *Nrf1*(b)-WT mice (Fig. 2B). In addition, fasting plasma insulin levels of age-matched male *Nrf1*(b)-KO mice were also significantly higher than those in either RIP-Cre control or *Nrf1*(b)-HET mice (Fig. 2C). The plasma levels of glucagon showed no significant difference among *Nrf1*(b)-KO, *Nrf1*(b)-HET, and *Nrf1*(b)-WT mice (Fig. 2D). As a comparison, fasting plasma insulin showed no significant difference between *Nrf2*(b)-WT and *Nrf2*(b)-KO male mice, which were developed by using the same RIP-Cre system as for *Nrf1*(b)-KO mice (Fig. 2C). These findings clearly demonstrated that the hyperinsulinemia observed in *Nrf1*(b)-KO mice is attributable to Nrf1 deficiency, rather than a result of the confounding effect of RIP-Cre integration. Homeostatic model assessment for insulin resistance (HOMA-IR) in male *Nrf1*(b)-KO mice was significantly higher than that in *Nrf1*(b)-WT mice (Supplementary Fig. S7). *Nrf1*(b)-KO female mice also tended to display a higher HOMA-IR level than *Nrf1*(b)-WT female mice (Supplementary Fig. S7). Intraperitoneal insulin tolerance test performed in three pairs age-matched female mice showed a trend that *Nrf1*(b)-KO mice are more insulin resistant (Supplementary Fig. S8).

Nrf1(b)-KO islets exhibited elevated basal insulin release but reduced GSIS

Protein expression of insulin and glucagon in pancreatic islets measured by immunostaining (Supplementary Fig. S9A) and relative protein content of insulin in whole pancreas (Supplementary Fig. S9B) were similar between the genotypes. The plasma insulin levels of *Nrf1*(b)-WT mice exhibited a robust response to acute glucose stimulation by showing a significant increase post glucose intraperitoneal injection (Fig. 3A). Interestingly, *Nrf1*(b)-KO mice that had elevated basal (fasting) plasma insulin levels essentially lost the responsiveness to glucose stimulation (Fig. 3A). This insulin response profile closely resembles pre-T2D conditions. In contrast, neither basal insulin release nor GSIS showed a significant difference between *Nrf2*(b)-WT and *Nrf2*(b)-KO mice generated by using the same RIP-Cre mice as in *Nrf1*(b)-KO mice (Fig. 3B). In agreement with the *in vivo* measurements, the mRNA (Fig. 3C) and protein (Fig. 3D) expression of insulin in isolated islets showed no significant difference between *Nrf1*(b)-KO and *Nrf1*(b)-WT mice. Although insulin secretion from cultured *Nrf1*(b)-KO

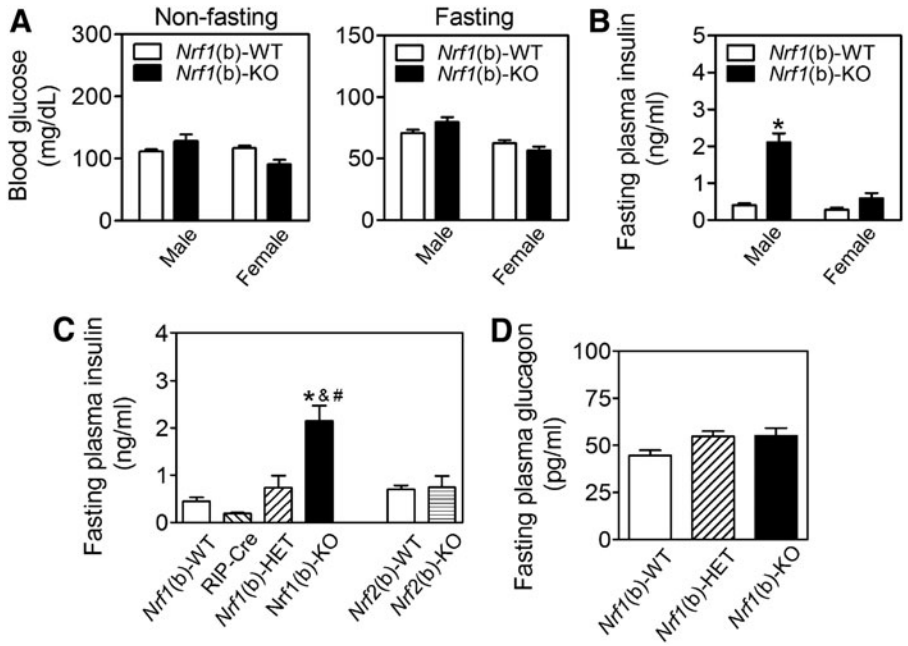

FIG. 2. *Nrf1*(b)-KO mice exhibit severe hyperinsulinemia. **(A)** Blood glucose levels under nonfasting (*left panel*) and fasting (*right panel*) conditions. $n = 9$–13 for nonfasting measurements; $n = 20$–27 for fasting measurements. Animal age is 11–17 weeks. **(B)** Fasting plasma insulin levels. $n = 9$–20. Animal age is 11–17 weeks. **(C)** Fasting plasma insulin levels in age-matched males. $n = 5$–17. Animal age is 11–12 weeks. $^{*}p < 0.05$ *versus Nrf1*(b)-WT. **(D)** Fasting plasma glucagon levels in males. $n = 8$–34. Animal age is 11–17 weeks. $^{*}p < 0.05$ *versus Nrf1*(b)-WT; $^{\#}p < 0.05$ *versus* RIP-Cre; $^{\&}p < 0.05$ *versus Nrf1*(b)-HET. KO, knockout.

islets under low-glucose (3 m*M*) condition was dramatically higher than that of *Nrf1*(b)-WT mice, the insulin secretion response of *Nrf1*(b)-KO islets to high glucose (16.7 m*M*) was very small. In contrast, there was no difference of KCl-triggered insulin release between genotypes (Fig. 3E). These *in vitro* results are similar to those found with MIN6 cells with all-isoform *Nrf1* knockdown (Fig. 1F).

Impaired insulin secretion induced by Nrf1 silencing is associated with altered glucose metabolism

Glycolysis and mitochondrial metabolism leading to accelerated ATP generation and increased ATP/ADP ratio are key signaling events in GSIS (16). To investigate the mechanism(s) by which *Nrf1* deficiency in β-cells leads to impaired insulin secretion, we first examined the metabolic

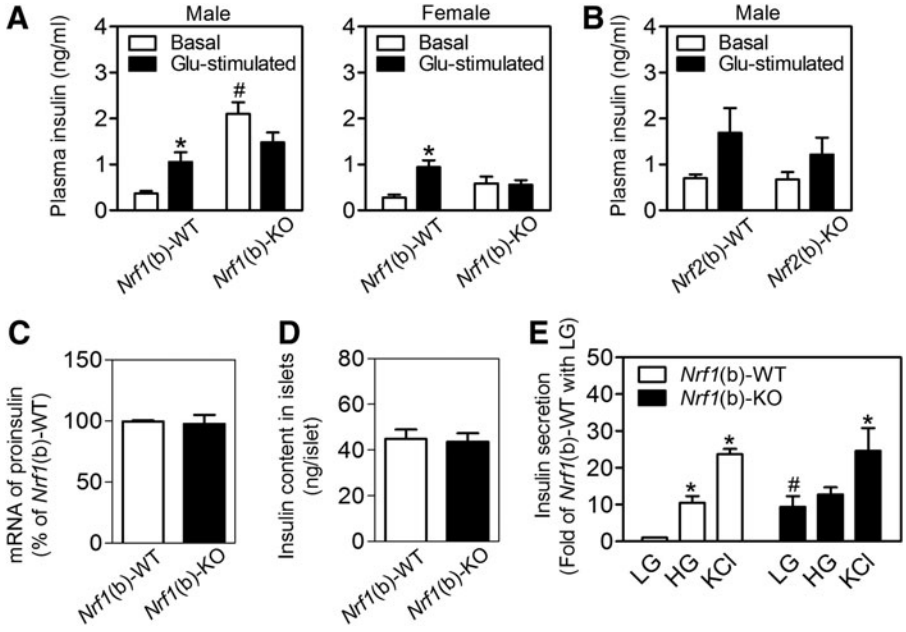

FIG. 3. Expression and secretion of insulin in *Nrf1*(b)-KO mice. Animal age is 11–17 weeks. **(A)** *In vivo* analysis of GSIS in *Nrf1*(b)-KO and *Nrf1*(b)-WT mice. Basal, fasting plasma insulin levels; Glu-stimulated, plasma insulin levels post glucose challenge (1.0 mg of glucose/g of BW; IP injection, 15 min). $n = 7$–20. $^{*}p < 0.05$ *versus* Basal of the same genotype; $^{\#}p < 0.05$ *versus Nrf1*(b)-WT under basal condition. **(B)** *In vivo* analysis of GSIS in *Nrf2*(b)-KO and *Nrf2*(b)-WT mice. Measurements were conducted under the same conditions as in **(A)**. $n = 6$–16. **(C)** mRNA expression of proinsulin in cultured islets. Isolated islets were cultured for 48 h before mRNA isolation. $n = 5$–6. **(D)** Insulin content in islets after a 48-h culture. $n = 14$. **(E)** GSIS in cultured islets. The levels of secreted insulin in 30 min were normalized by DNA content. LG, low glucose (3 m*M*); HG, high glucose (16.7 m*M*); KCl, 30 m*M* potassium chloride. $n = 4$–12. $^{*}p < 0.05$ *versus* LG of the same genotype; $^{\#}p < 0.05$ *versus Nrf1*(b)-WT with LG. GSIS, glucose-stimulated insulin secretion.

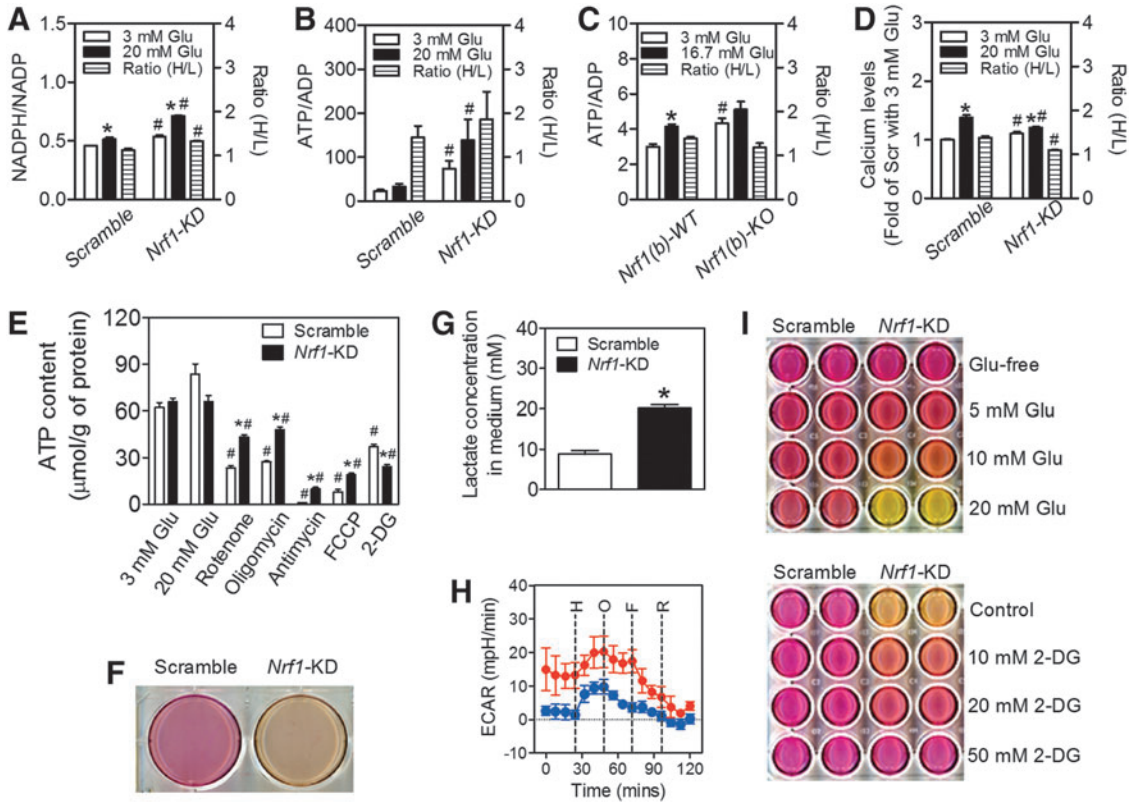

FIG. 4. Effects of *Nrf1* silencing on glucose metabolism and ATP production in MIN6 β-cells and isolated mouse islets. (A, B, D) NADPH/NADP ratio **(A)**, ATP/ADP ratio **(B),** and calcium levels **(D)** in MIN6 cells. Cells were treated with 3 and 20 m*M* glucose (Glu) for 30 min followed by immediate analyses. Ratio (H/L), ratios of NADPH/NADP, ATP/ADP or calcium level under 20 m*M* Glu over 3 m*M* Glu condition. $n=4$. $^{*}p<0.05$ *versus* Scramble with 3 m*M* Glu. $^{\#}p<0.05$ *versus* Scramble with the same Glu condition. **(C)** ATP/ADP ratio in cultured mouse islets. Cultured (48 h) islets were treated with 3 and 16.7 m*M* Glu for 30 min followed by an immediate analysis of ATP/ADP ratio. Ratio (H/L), ATP/ADP under 16.7 m*M* Glu over 3 m*M* Glu. $n=6$. $^{*}p<0.05$ *versus Nrf1*(b)-WT islets with 3 m*M* Glu. $^{\#}p<0.05$ *versus Nrf1*(b)-WT islets with the same concentration of Glu. **(E)** ATP levels measured under glucose (3 or 20 m*M* Glu), rotenone (1 μ*M*), oligomycin (1 μ*M*), antimycin (50 ng/ml), FCCP (1 μ*M*), or 2-DG (100 m*M*) in Kreb's buffer with 3 m*M* Glu. $n=3$–15. $^{*}p<0.05$ *versus* Scramble cells with the same treatment; $^{\#}p<0.05$ *versus* the same cells with 3 m*M* Glu. **(F)** Representative image of acidification of culture media in *Nrf1*-KD cells. Confluent cells were cultured in normal growth media for 48 h. **(G)** Lactate levels in culture media. $n=6$. $^{*}p<0.05$ *versus* Scramble. **(H)** Representative results of ECAR measured by a Seahorse XF24 analyzer. Measurement was started in Kreb's buffer with 3 m*M* glucose followed by subsequent addition of 20 m*M* glucose **(H)**, 1 μ*M* oligomycin (O), 1 μ*M* FCCP (F), and 1 μM rotenone (R). $n=3$–4. **(I)** *Upper panel*, acidification of culture media of *Nrf1*-KD MIN6 cells is dependent on glucose. Confluent cells were cultured in DMEM media with different concentrations of glucose (Glu) for 48 h; *Lower panel*, glycolytic inhibition rescues the acidification of culture media of *Nrf1*-KD MIN6 cells. Confluent cells were cultured in normal growth media (20 m*M* glucose) with different concentrations of 2-DG for 48 h. 2-DG, 2-deoxy-D-glucose; DMEM, Dulbecco's modified Eagle's medium; ECAR, extracellular acidification rate; FCCP, trifluorocarbonylcyanide phenylhydrazone. To see this illustration in color, the reader is referred to the web version of this article at www.liebertpub.com/ars

profiles of *Nrf1*-KD MIN6 cells and *Nrf1*(b)-KO mouse islets. As shown in Figure 4A–C, *Nrf1*-KD MIN6 cells and/or *Nrf1*(b)-KO islets displayed substantially increased NADPH/NADP ratio and ATP/ADP ratio under basal (low glucose) conditions. In addition, intracellular calcium levels in *Nrf1*-KD MIN6 cells in response to glucose stimulation displayed a pattern similar to the ATP/ADP ratio, showing elevated basal level and reduced response to glucose stimulation (Fig. 4D). These findings may particularly explain the elevated basal insulin secretion observed in *Nrf1* deficiency MIN6 cells and islets (Figs. 1F and 3E). Compared with Scramble cells, the ATP production of *Nrf1*-KD MIN6 cells had almost no response to high glucose challenge (Fig. 4E). When mitochondrial oxidation was blocked with various agents, there was less reduction in ATP content in *Nrf1*-KD MIN6 cells than that in Scramble cells (Fig. 4E). Thus, mitochondrial oxidative phosphorylation may not contribute as much to total ATP when *Nrf1* is deleted. Interestingly, glycolysis may be a more significant source of ATP production in *Nrf1*-KD cells, because inhibition of glycolysis with 2-deoxy-D-glucose (2-DG) suppressed ATP production in *Nrf1*-KD cells to a greater extent than in Scramble cells (Fig. 4E). In addition, *Nrf1*-KD cells may have higher glycolysis, since *Nrf1*-KD cells exhibited a dramatic acidic pH change in the culture medium (Fig. 4F), increased lactate production (Fig. 4G) and increased basal (3 m*M* glucose) extracellular acidification rate (ECAR) as measured by a Seahorse XF24 analyzer (Fig. 4H). Moreover, the pH change in the culture media of *Nrf1*-KD

cells was positively correlated with the concentrations of glucose in the media and was sensitive to 2-DG inhibition of glycolysis (Fig. 4I). To further define the effect of *Nrf1* silencing on β-cell metabolism, mitochondrial respiration was evaluated by measuring oxygen consumption rate (OCR) in MIN6 cells. As shown in Supplementary Figure S10A, *Nrf1*-KD cells exhibited a dramatically increased OCR under basal (3 m*M* glucose) and high-glucose conditions. The OCR in both Scramble and *Nrf1*-KD cells was significantly suppressed by mitochondrial complex inhibitors (oligomycin and rotenone), but not by glycolytic blocker (2-DG). Importantly, the reduction in *Nrf1*-KD cells was more dramatic than that in Scramble cells (Supplementary Fig. S10A, B), suggesting that the augmented OCR in *Nrf1*-KD cells is associated with enhanced mitochondrial metabolism.

Aberrant expression of glycolytic proteins in Nrf1-KD MIN6 cells

GSIS is closely coupled to glucose uptake, metabolism, and ATP production in pancreatic β-cells (15). Consistent with the glucose metabolic and insulin secretion profile described earlier, *Nrf1*-KD MIN6 cells expressed enhanced levels of glucose transporter 2 (GLUT2), lactate dehydrogenase 1 (LDH1), glyceraldehyde 3-phosphate dehydrogenase (GAPDH), and hexokinase 1 (HK1) (Fig. 5A, B). In contrast, glucokinase (GCK, also known as HK4) is decreased (Fig. 5A, B). As seen with the *Nrf1*-KD MIN6 cells, expression of HK1 in *Nrf1*(b)-KO islets also tended to increase compared with *Nrf1*(b)-WT islets (Supplementary Fig. S11). Other factors related to cellular metabolism, including expression of p53 and phosphorylation of AKT and AMP-activated protein kinase α (AMPKα), appeared to be upregulated (Supplementary Fig. S12) in *Nrf1*-KD MIN6 cells. As expected with elevated protein expression of GLUT2 and LDH1, *Nrf1*-KD cells also had significantly increased glucose uptake (Fig. 5C) and LDH activity (Fig. 5D). Silencing of *Nrf1* did not affect mitochondrial proteins, including complex I (MTCO1), complex II (MTCO2), cytochrome c (CYC), gamma subunit of ATP synthase F1 complex (ATPase), and mitochondrial biogenesis-related factors, for example, peroxisome proliferator-activated receptor gamma coactivator 1α (PGC1α), PGC1β, and nuclear respiratory factor 1 (Fig. 5E and Supplementary Fig. S13). Knockdown of *Nrf1* also did not alter mitochondrial mass (Fig. 5F).

In agreement with the findings in MIN6 cells, stable knockdown of *Nrf1* in another β-cell line, β-TC6 insulinoma cells, also resulted in significant increases in *Hk1* mRNA expression, ECAR, and basal insulin release (Supplementary Fig. S14). Of note, the basal expression of *Hk1* in β-TC6 cells is much higher than that in MIN6 cells, which may be associated with the reduced GSIS in β-TC6 cells.

Silencing of HK1 rescues the impaired glycolysis and GSIS in Nrf1-KD MIN6 cells

Mannose and fructose, but not galactose, are, similar to glucose, substrates of HK and may enter the glycolysis pathway directly as fructose-6-phosphate. The insulin secretion profile of *Nrf1*-KD cells in response to glucose, mannose, fructose, and galactose (Fig. 1F and Supplementary Fig. S3) suggests that induction of *Hk1* by *Nrf1* silencing may be a key event underlying the phenotype. To further test the hypothesis that Nrf1 deficiency-induced expression of *Hk1* is responsible for the altered glucose metabolism and insulin secretion in pancreatic β-cells, we determined the effect of silencing *Hk1* in *Nrf1*-KD MIN6 cells on glycolysis and GSIS. One of the five lentiviral shRNAs against mouse *Hk1* markedly attenuated the protein expression of HK1 in *Nrf1*-KD cells, but did not affect GLUT2, GCK, and LDH (Fig. 6A). Importantly, the impairment of ECAR and insulin secretion of *Nrf1*-KD cells was substantially reversed by *Hk1* silencing (Fig. 6B–D). In addition, glycolysis appears to be a primary contributor to the enhanced basal insulin release in these cells because glycolytic inhibitor 2-DG caused a dose-dependent suppression on basal insulin release in *Nrf1*-KD MIN6 cells (Fig. 6E). Our results

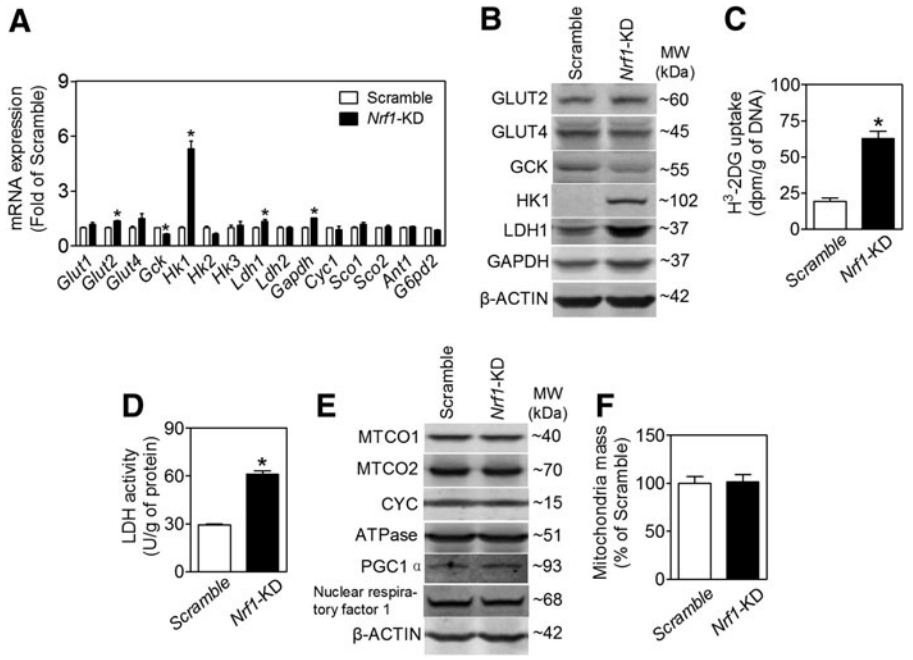

FIG. 5. Effects of *Nrf1* silencing on expression and activity of glycolytic enzymes and mitochondrial proteins in MIN6 β-cells and mouse islets. (A) mRNA expression in MIN6 cells. $n = 6$–18. $^*p < 0.05$ *versus* Scramble. **(B)** Representative images of immunoblotting. $n = 2$–6. **(C)** Glucose uptake in MIN6 cells determined by the accumulation of [^{3}H]-2-DG in 30 min. $n = 6$. $^*p < 0.05$ *versus* Scramble. **(D)** Cellular LDH activity in MIN6 cells. $n = 12$. $^*p < 0.05$ *versus* Scramble. **(E)** Immunoblotting of mitochondrial proteins. $n = 2$–6. **(F)** Mitochondria mass measured by Flow cytometry with MitoTracker green. $n = 4$–6. LDH, lactate dehydrogenase.

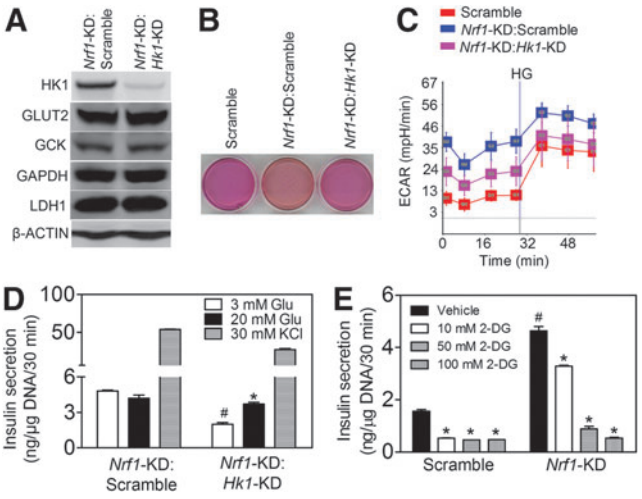

FIG. 6. Effects of *Hk1* silencing on glycolysis and insulin secretion in *Nrf1*-KD MIN6 cells. **(A)** Protein expression of HK1 and glycolysis-related proteins. *Nrf1*-KD:Scramble, *Nrf1*-KD cells transduced with scramble shRNA; *Nrf1*-KD:*Hk1*-KD, *Nrf1*-KD cells transduced with shRNA against *Hk1*. $n=3$. **(B)** Representative image of pH changes of culture media. Confluent cells were cultured for 48 h. **(C)** ECAR measured in Kreb's buffer with 3 m*M* glucose followed by addition of 20 m*M* glucose (HG). $n=3$–4. **(D)** Insulin secretion. Glu, glucose. $n=4$–6. $^{*}p<0.05$ *versus* 3 m*M* Glu of *Nrf1*-KD:*Hk1*-KD cells; $^{\#}p<0.05$ *versus Nrf1*-KD:Scramble cells with 3 m*M* Glu. **(E)** Glycolytic inhibition suppresses basal insulin release in MIN6 cells. Scramble and *Nrf1*-KD MIN6 cells were incubated with 2-DG in Kreb's buffer with 3 m*M* Glu. $n=4$. $^{*}p<0.05$ *versus* the same cells with 3 m*M* Glu; $^{\#}p<0.05$ *versus* Scramble with the same treatment. HK1, hexokinase 1. To see this illustration in color, the reader is referred to the web version of this article at www.liebertpub.com/ars

here indicate that increased HK1 resulting from silencing of *Nrf1* is one of the critical downstream events affecting glucose metabolism and GSIS in MIN6 cells.

Discussion

We found that deficiency of *Nrf1* in pancreatic β-cells disrupts glucose metabolism and ATP production in the cells and impairs insulin secretion leading to pre-T2D-like metabolic disorders. Specifically, *Nrf1*-KD β-cells displayed elevated basal insulin release, decreased GSIS, and altered glucose metabolism. The alteration included enhanced glucose uptake and aerobic glycolysis, with upregulation of relevant metabolic enzymes, including GLUT2, HK1, and LDH1. In contrast, the GCK, the predominant form of HKs that phosphorylate glucose in β-cells (17, 39), was significantly downregulated. In agreement with the findings in MIN6 cells, *Nrf1*(b)-KO islets also showed enhanced basal insulin release and reduced GSIS. *Nrf1*(b)-KO mice exhibited severe fasting hyperinsulinemia and glucose intolerance. These findings strongly suggest that loss of functional Nrf1 in β-cells may be a risk factor in the development of T2D.

Insulin secretion from β-cells is primarily controlled by glucose, with some contributions from metabolic, neural, hormonal, and pharmacological factors. Proper GSIS requires coordinating glucose uptake, glycolysis, mitochondrial metabolism, cell membrane depolarization, calcium influx, and insulin exocytosis (16). This coordination is subject to a very tight control by many signaling pathways (18): glycolysis and mitochondrial oxidative phosphorylation leading to accelerated ATP generation are two of the most important (16, 28). Glycolysis involves high-affinity HKs and low-affinity GCK in most mammalian cells (30). Because the expression levels of high-affinity HKs are very low in islet β-cells, the low-affinity GCK serves as the primary kinase controlling the rate-limiting step of glycolysis in β-cells (4, 15, 16, 39). In addition, LDH, the enzyme that catalyzes the interconversion of pyruvate and lactate and their co-substrates NADH and NAD^+ is also expressed at low levels in β-cells (39). In this manner, high fractions of pyruvate, generated through glycolysis in the cells, go to the mitochondria for oxidation through the tricarboxylic acid cycle (1). Tight coupling between glycolysis and mitochondrial oxidation of pyruvate is required for robust insulin secretion (1, 31). This coupling is the reason that forced overexpression of HK1 in β-cells perturbs glycolysis and mitochondrial metabolism, leading to impaired basal insulin release and GSIS (4, 5). Acute overexpression of LDH1 also impairs β-cell mitochondrial metabolism and insulin secretion (1). Nonetheless, not all the factor(s) that coordinate glycolysis and mitochondrial oxidative phosphorylation in β-cells are completely defined. This study demonstrates that loss of *Nrf1* results in a dramatically enhanced glycolysis and impaired insulin secretion. In these cells ATP production is largely dependent on the augmented glycolysis rather than mitochondrial oxidation. ATP production in *Nrf1*-KD MIN6 cells was less sensitive to mitochondrial complex blockers but more sensitive to glycolytic inhibition. Since silencing of *Hk*1 normalized most of the phenotypes of *Nrf1*-KD MIN6 cells, the aberrant expression of HKs (*e.g.*, dramatic induction of high-affinity HK1 and repression of low-affinity GCK) is likely responsible for the elevated glycolysis and reduced responsiveness to glucose (Fig. 7). Uncovering the detailed mechanisms of how Nrf1 modulates the expression of HKs will require further study. With regard to the enhanced OCR in *Nrf1*-KD cells, our measurements revealed that OCR, but not EACR, can be significantly reduced by inhibition of AMPK or β-oxidation (Supplementary Fig. S15), suggesting that β-oxidation and AMPK activity may be upregulated in the cells and partially responsible for their enhanced OCR. However, the mechanistic details behind the phenotype still need further investigation.

Due to alternative RNA splicing, translation, and/or proteolysis, Nrf1 exists as peptides of varying size. At this juncture, we do not understand the expression, function, and tissue distribution of various isoforms of Nrf1. Long isoforms of Nrf1 (L-Nrf1s, 742, 761, and 772 aa in human; 741 and 742 aa in mouse) are modified in the ER and in coordination with Nrf2 regulate cellular adaptive antioxidant response *via* ARE (6, 24, 49, 50). In addition, L-Nrf1s play a crucial role in proteasome homeostasis by regulating ARE-dependent proteasomal genes (37, 40). More recently, Kwong *et al.* found that Nrf1b (584 aa in human; 583 or 572 aa in mouse) is targeted to the nucleus where it activates ARE-genes (23). In contrast, Nrf1-p65 (447 aa in human; 453 aa in mouse) is a dominant negative regulator of ARE-mediated transcription (42). Since L-Nrf1s regulate the transcription of multiple antioxidant enzymes involved in GSH synthesis and ROS

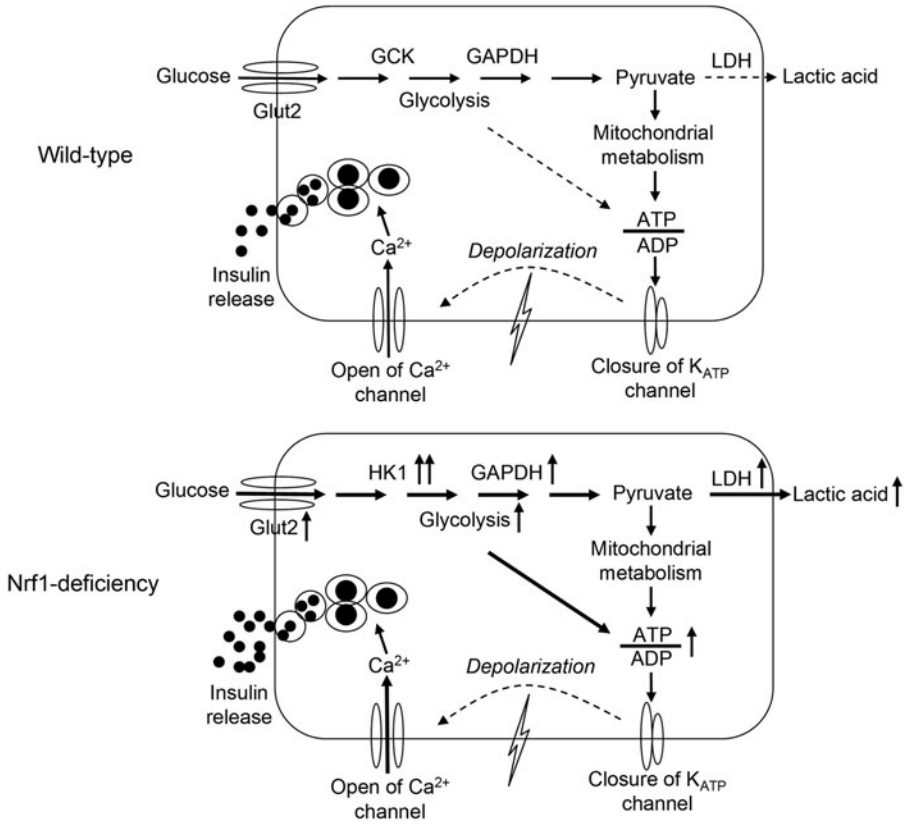

FIG. 7. Postulated mechanisms regarding pancreatic β-cell dysfunction caused by *Nrf1* deficiency. *Upper panel*: Proper GSIS requires coordinating glucose uptake, glycolysis, mitochondrial metabolism, cell membrane depolarization, calcium influx, and insulin exocytosis. Levels of HK1, 2, and 3 that have high affinities for glucose are low in normal islet β-cells. The absence of high-affinity HKs allows low-affinity GCK to serve as the primary enzyme regulating the rate-limiting step of glycolysis, thereby making β-cells more responsive to changes in glucose levels. *Lower panel*: *Nrf1* deficiency in the β-cell results in induction of multiple glucose-metabolizing enzymes, including *Glut2*, *Hk1, Gapdh*, and *Ldh1*, leading to elevated glycolysis and lactate production. The aberrant expression of glucose metabolic enzymes, in particular HK1 overexpression, in the β-cell alters its responsiveness to changes in glucose levels, leading to elevated basal insulin release but reduced GSIS. GCK, glucokinase.

detoxification (6, 24, 49, 50), reduction of intracellular GSH and elevated accumulation of ROS in *Nrf1*-KD cells may be attributed to the absence of L-Nrf1s. In addition, Nrf1 silencing-induced alteration in mitochondrial metabolism may also affect cellular redox homeostasis. Importantly, silencing of all isoforms, but not long isoforms-specific knockdown (Supplementary Fig. S16), resulted in impaired β-cell function. One or more of the multiple short isoform(s) of Nrf1 may play fundamental roles in regulating glucose metabolism and glucose sensing in β-cells. However, isoform(s) of Nrf1 that regulates these processes is not known.

The RIP-Cre mice, where a short fragment of the rat insulin II gene promoter controls Cre recombinase, have been widely used to generate β-cell-specific KO mice (29, 43), and more recently, brain-specific silencing (22). While most of the studies using pancreatic β-cell-specific KO mice derived from RIP-Cre line demonstrated pronounced glucose metabolism phenotypes, the RIP-Cre mice alone display glucose intolerance and impaired insulin secretion (26). Thus, integration or expression of Cre recombinase itself may be responsible for some of the phenotypes initially thought to be caused by gene targeting. This concern is particularly worrisome in the studies without RIP-Cre mice as controls. Since RIP-Cre is also expressed in some neurons (22), caution should be taken regarding the systemic parameters that could be influenced not just by the operation of islets but also of central nervous system.

In this study, we found that *Nrf1*(b)-KO, but not *Nrf1*-flox knock-in (KI), RIP-Cre alone or even *Nrf1*(b)-HET mice, developed severe hyperinsulinemia. In contrast, *Nrf2*(b)-KO mice, which were developed by using the same RIP-Cre mice as in *Nrf1*(b)-KO line, showed no increased levels of fasting plasma insulin. Thus, the hyperinsulinemia observed in *Nrf1*(b)-KO mice is due to disruption of *Nrf1* in pancreatic β-cells, even though the potential contribution of hypothalamus to the phenotype cannot be fully excluded. Of note, hyperinsulinemia is widely considered a compensatory response to insulin resistance, and prolonged hyperinsulinemia *per se* can induce insulin resistance and obesity (7, 9, 32). The hyperinsulinemia observed in *Nrf1*(b)-KO mice may, at least in part, account for their glucose intolerance.

In contrast to normal differentiated cells, most cancer cells rely on aerobic glycolysis to generate ATP (27). This shift from oxidative phosphorylation to glycolysis for energy by cancer cells is called the Warburg effect. Multiple TFs, including p53, AKT, mammalian target of rapamycin, hypoxia-induced factor 1α (HIF1α), and AMPK, may contribute to the altered glucose metabolism in cancer cells (27). Interestingly, because the expression of phosphorylated AKT, p53, and phosphorylated AMPKα trended higher in *Nrf1*-KD MIN6 cells, these proteins may be involved in *Nrf1* deficiency-induced alteration of glucose metabolism in β-cells. In light of the importance of the Warburg effect in cancer biology, studies on the regulatory role of Nrf1 in β-cell metabolism and glucose sensing are likely to enhance our understanding of cancer cell proliferation control.

The biochemical mechanism underlying insulin secretion and β-cell toxicity has been extensively studied with the aim of identifying therapeutic targets for diabetes for decades. Although several concepts have been developed and targets have been identified, the progress to improve β-cell function and/or survival made so far clearly does not meet the clinical demands in the face of the rapidly increasing prevalence of diabetes. This study shows the critical roles of Nrf1 in

regulating the coupling of glycolytic and mitochondrial metabolism and of controlling insulin secretion in pancreatic β-cells. These findings suggest that Nrf1 and its regulated pathways may be novel pharmacological targets to improve the function of insulin-secreting β-cells.

Materials and Methods

Cell culture and reagents

MIN6 cells were kindly provided by Dr. Marcia Haigis (Harvard University, Boston, MA) and maintained in Dulbecco's modified Eagle's medium (DMEM) containing 25 m*M* glucose, with 15% fetal bovine serum (FBS), 100 U/ml penicillin, 100 μg/ml streptomycin, 2 m*M* L-glutamine, and 5 μl/L β-mercaptoethanol in humidified 5% CO_2, 95% air at 37°C. Culture media, FBS, phosphate-buffered saline (PBS, pH 7.4), and supplements were purchased from Life Technologies (Carlsbad, CA). β-Mercaptoethanol, D-(+)-glucose, mannose, fructose, galactose, rotenone, oligomycin, antimycin, trifluorocarbonylcyanide phenylhydrazone (FCCP), and 2-DG were obtained from Sigma (St. Louis, MO).

Lentiviral-based shRNA transduction

MISSION shRNA lentiviral vectors were obtained from Sigma and lentiviral particles were prepared by using the manufacturer's protocol. Lentiviral transduction of MIN6 cells with particles for shRNAs targeting mouse *Nrf1* (SHVRSNM_008686) or Scrambled nontarget negative control (SHC002V) was performed as previously described (49).

Measurements of intracellular GSH, ROS, and calcium

Intracellular levels of GSH and GSSG were measured immediately after cell collection using a BIOXYTECH GSH/GSSG-412 kit (OxisResearch, Portland, OR) according to the manufacturer's protocol (34). ROS levels were measured by flow cytometry using the fluorescent probe 5-(and-6)-chloromethyl-2′,7′-dichlorodihydrofluorescein diacetate, acetyl ester (CM-H2DCFDA; Life Technologies) as previously described (35). Intracellular calcium in MIN6 cells were measured using a calcium indicator Fluo-4 AM (Life Technologies) in a 96-well plate. After a 30 min incubation with 4 μ*M* of Fluo-4 in Kreb's buffer with 3 m*M* or 20 m*M* glucose, the fluorescence intensity of cells was determined by a FlexStation 3 Multi-Mode Microplate reader (Ex: 494 nm, Em: 516 nm; Molecular Devices, Sunnyvale, CA).

Mice

Nrf1(b)-KO mice were developed by crossing the mice bearing an $Nrf1^{flox}$ allele (33) and Ins2-Cre:B6.Cg-Tg(Ins2-cre)25Mgn/J (RIP-Cre) mice (#003573; Jackson Laboratories, Bar Harbor, ME), which specifically express Cre recombinase in pancreatic β-cells. To generate *Nrf1*(b)-KO mice, $Nrf1^{flox/flox}$ KI males were crossed with RIP-Cre-positive females. Resulted $Nrf1^{flox/-}$:RIP-Cre-positive mice were crossed with $Nrf1^{flox/flox}$ KI to generate breeders with a genotype of $Nrf1^{flox/flox}$:RIP-Cre-positive mice. Approximately five pairs of $Nrf1^{flox/flox}$ KI:RIP-Cre-positive breeders were kept to the end of the project. Resulting *Nrf1*(b)-KO mice with a genotype of $Nrf1^{flox/flox}$ KI:RIP-Cre-positive and their wild-type littermates ($Nrf1^{flox/flox}$ KI:RIP-Cre-negative), and RIP-Cre-positive were used in this study. Similarly, pancreatic β-cell-specific *Nrf2* knockout [*Nrf2*(b)-KO] mice were generated by using the RIP-Cre mice and $Nrf2^{loxP/loxP}$ KI mice previously developed (45). Genotyping was performed by PCR (primer sequences in Supplementary Table S1) using genomic DNA that was isolated from tail snips as previously detailed (33, 45). The mice were housed four per cage in virus-free facilities on a 12-h light/12-h dark cycle, fed an NIH07 chow diet (Zeigler Brothers, Gardners, PA), and provided reverse osmosis water *ad libitum*. Food intake, water consumption, and body weight were measured weekly. Feed efficiency (grams gained per kilocalorie consumed) was determined per individual mouse. All protocols for animal use were approved by the Institutional Animal Care and Use Committees of The Hamner Institutes and China Medical University, and they were in accordance with the National Institutes of Health guidelines.

Measurements of blood glucose and plasma insulin

Nonfasting and fasting (16 h) blood samples collected from tail bleeds were immediately analyzed for glucose by using the FreeStyle Blood Glucose Monitoring System (TheraSense, Inc., Alameda, CA). For plasma isolation and tissue collection, animals were euthanized by CO_2 exposure. Plasma insulin was measured by using the Sensitive Rat Insulin radioimmunoassay (RIA) kit as previously described (34).

Measurements of GSIS in vivo *and* in vitro

Plasma insulin levels were measured under basal and glucose-stimulated conditions. After a 16-h overnight fasting, mice were given either D-(+)-glucose (1 g/kg body weight) in saline or saline alone. At exactly 15 min post glucose administration, the mice were euthanized by CO_2 exposure, followed by blood and tissue collection. Plasma insulin was measured as detailed earlier. For the *in vitro* GSIS assay, pancreatic islets were isolated from 10- to 14-week-old mice by collagenase P (Roche, Basel, Switzerland) digestion and cultured as described previously (34). Before GSIS measurement, isolated islets were cultured 48 h in RPMI 1640 media supplemented with 10 m*M* glucose, 10% FBS, 2 m*M* L-glutamine, 100 U of penicillin/ml, and 100 μg of streptomycin/ml. Measurements of insulin secretion were performed in static incubation condition as previously detailed (34).

Intraperitoneal glucose tolerance test

Intraperitoneal glucose tolerance test (IPGTT) was performed as previously described (45). Briefly, after 16-h fasting, animals received D-(+)-glucose (G8769, 1 g/kg body weight; Sigma) by intraperitoneal injection. At 15, 30, 60, and 120 min after glucose administration, glucose levels in blood collected from tail bleeds were analyzed immediately as detailed earlier.

Immunohistochemistry

Pancreas were fixed, embedded in paraffin, sectioned, and stained as previously described (45). The following primary antibodies against insulin (#15848-1-AP, 1:10,000; Proteintech Group, Inc., Chicago, IL), glucagon (#15954-1-AP, 1:20,000; Proteintech Group, Inc.), and HK1 (#2024, 1:800; Cell Signaling Technology, Inc., Danvers, MA) were used for the staining.

Reverse transcription–polymerase chain reaction

RNA isolation and quantitative real-time PCR (qPCR) were performed as previously described (45). A SensiFAST SYBR Hi-ROX kit (Bioline USA, Inc., Taunton, MA) and an AccuPower HotStart PCR PreMix system (Bioneer, Alameda, CA) were used for qPCR and regular PCR, respectively. The primers were designed by using Primer Express 4 (Applied Biosystems, Waltham, MA) and synthesized by Bioneer, Inc. (Alameda, CA). The primer sequences for qPCR and PCR for diverse isoforms of *Nrf1* are listed in Supplementary Tables S2 and S3, respectively. Real-time fluorescence detection was performed by using an ABI PRISM 7900HT Fast Real-time PCR System (Applied Biosystems). The cycling conditions of regular PCR for diverse isoforms of *Nrf1* were 94°C for 5 min followed by 35 cycles of 94°C for 30 s, 55°C or 65°C for 30 s, and 72°C for 30 s with a final extension of 72°C for 10 min. Expression levels of *18S* were used as loading controls. The PCR products stained with the SYBR Safe (Life Technologies) were separated by a gel electrophoresis with a 2.0% agarose gel.

Immunoblot analysis

Isolation of cell fractions and Western blotting were performed as previously described (45). Antibodies for GLUT4 (#2213, 1:1000), HK-1 (#9711, 1:1000), LDHA (#2012, 1:1000), PGC1α (#2178, 1:500), p-AKT(T308) (#4056, 1:1000), p-AKT(S473) (#9271, 1:1000), Total AKT (#4685, 1:1000), p-PTEN(S380) (#9551, 1:1000), p-AMPK (Thr172) (#2531, 1:1000), AMPK (#2532, 1:1000), p-PDK1 (#3438, 1:1000), and p-PKC (#9371, 1:1000) were purchased from Cell Signaling Technology, Inc. Antibodies against GLUT2 (sc-9117, 1:500), GCK (sc-7908, 1:500), GAPDH (sc-20357, 1:500), ATPase (sc-33618, 1:500), NRF1 (sc-33771, 1:500), P53 (sc-6243, 1:250), and INSULIN (sc-9168, 1:500) were purchased from Santa Cruz, Inc. (Santa Cruz, CA). Antibody for β-Actin (A1978, 1:2000) and HIF1α (H6536, 1:1000) were purchased from Sigma. Antibodies for MTCO1 (459100, 1:1000) and MTCO2 (459200, 1:1000) were from Invitrogen (Life Technologies). Antibody for CYC (556433, 1:1000) was purchased from BD (Becton Dickinson, San Jose, CA). The MW of each protein shown on the immunoblot was estimated based on the MagicMark™ XP Western Protein Standard (Invitrogen) on 12% Tris-Glycine gels (Invitrogen). Quantification of the results was performed with Bio-Rad Quantity One 1-D analysis software (Bio-Rad Laboratories, Hercules, CA).

Measurements of ATP level and ATP/ADP ratio

Cells or islets were washed thrice with ice-cold Kreb's buffer containing the same concentrations of glucose as various treatments and lysed in 1% trichloroacetic acid followed by centrifugation at 12,000 *g* for 5 min. Resulting supernatants were used immediately for measurement of ATP and ATP/ADP ratio by using the ATP Bioluminescent Assay Kit (Sigma) and ATP/ADP Ratio-Glo™ Assay kit (Promega, Madison, WI), respectively, as per the manufacturer's protocols.

Measurement of ECAR and OCR in MIN6 cells

ECAR and OCR were measured by using the XF24 Extracellular Flux Analyzer (Seahorse Bioscience, Billerica, MA) as previously described (13). MIN6 cells were seeded in XF24-well microplates (Seahorse Bioscience) at 1.0×10^5 cells per well in 200 μl medium and cultured at 37°C/5% CO_2 overnight. Assays were initiated by replacing the growth medium from each well with 600 μl prewarmed Kreb's buffer (3 m*M* glucose) followed by additions of various reagents as detailed in the legends of Figures 4H, 6C and Supplementary Figure S10A. ECAR and OCR were calculated by using Extracellular Flux Analyzer software based on pH changes and oxygen tension, respectively. At least three independent experiments were performed, and data showed in figures are representative results.

Lactate measurement

Lactate levels in medium were determined by using a commercial lactate assay kit (BioVision, Mountain View, CA) based on an enzymatic reaction catalyzed by lactate oxidase and interaction of the product with a probe to produce fluorescence (at excitation/emission = 535/590 nm). The concentration of each sample was calculated by using a standard curve.

LDH activity

Cells were washed twice with ice-cold PBS and lysed in cold PBS by sonication, followed by centrifugation at 12,000 *g* for 5 min. The resulting supernatants were used immediately for measurement of LDH activity by using a CytoTox 96® Non-Radioactive Cytotoxicity Assay kit (Promega). Briefly, 5 μl of cell lysates (1 μg protein/μl) or LDH standards were incubated with 45 μl PBS (containing 0.5% bovine serum albumin [BSA]) and 50 μl LDH Assay buffer for 30 min in a 96-well plate. After an 1-h incubation with stop solution, the absorbance was determined at 590 nm. Protein concentrations were determined by a Bicinchoninic acid (BCA) protein assay kit (Thermo Scientific Pierce, Rockford, IL) by using BSA as a standard.

Glucose uptake assay

Glucose uptake in MIN6 cells was measured in Kreb's buffer containing 3 m*M* glucose as previously described (46). Briefly, MIN6 cells plated in a 12-well plate were preincubated in Kreb's buffer for 30 min. Subsequently, the cells were incubated with 0.15 μCi [^{3}H]-2-deoxy-D-glucose ([^{3}H]-2-DG; PerkinElmer, Inc., Waltham, MA) in 1 ml of Kreb's buffer. After a 2-h incubation, the radioactivity of cell lysates was determined in 5 ml of Ecolume (MP Biomedicals, LLC, Solon, OH) by using Tri-carb Liquid Scintillation Analyzer (Packard Instrument Co., Inc., Meriden, CT). The reading, after subtracting the nonspecific binding of [^{3}H]-2-DG with cell surface, was normalized with DNA content.

Statistical analysis

All statistical analysis was performed by using Graphpad Prism 4 (GraphPad Software, San Diego, CA), with $p < 0.05$ considered significant. More specific indices of statistical significance are indicated in individual figure legends (Figs. 1–6 and Supplementary Figs. S3, S4, S5, S6, S7, S10, S14, S15, S16). Data are expressed as mean ± standard error of the mean. For comparisons between two groups, a Student's *t*-test was performed. For comparisons among multiple groups, one-way or two-way ANOVA with Bonferroni *post hoc* testing was performed.

Acknowledgments

This work was supported in part by National Institutes of Health Grant ES016005 (J.P.), Startup Funding of China Medical University (J.P.), Liaoning Pandeng Scholar Program (J.P.), Chinese Nature Science Foundation 81102156 (R.Z.) and 81372943 (R.Z.), and the Key Laboratory of Public Health Safety (Fudan Univeristy), Ministry of Education, China GW2014-1 (J.F.). The authors thank Lisa H. Webb (The Hamner Institutes), Carol Bobbitt (The Hamner Institutes), Yongyong Hou (China Medical University), and Yuanyuan Xu (China Medical University) for their careful management of animal care and breeding.

Author Disclosure Statement

No competing financial interests exist.

References

1. Ainscow EK, Zhao C, and Rutter GA. Acute overexpression of lactate dehydrogenase-A perturbs beta-cell mitochondrial metabolism and insulin secretion. *Diabetes* 49: 1149–1155, 2000.
2. Ashcroft FM and Rorsman P. Diabetes mellitus and the beta cell: the last ten years. *Cell* 148: 1160–1171, 2012.
3. Back SH and Kaufman RJ. Endoplasmic reticulum stress and type 2 diabetes. *Annu Rev Biochem* 81: 767–793, 2012.
4. Becker TC, BeltrandelRio H, Noel RJ, Johnson JH, and Newgard CB. Overexpression of hexokinase I in isolated islets of Langerhans *via* recombinant adenovirus. Enhancement of glucose metabolism and insulin secretion at basal but not stimulatory glucose levels. *J Biol Chem* 269: 21234–21238, 1994.
5. Becker TC, Noel RJ, Johnson JH, Lynch RM, Hirose H, Tokuyama Y, Bell GI, and Newgard CB. Differential effects of overexpressed glucokinase and hexokinase I in isolated islets. Evidence for functional segregation of the high and low Km enzymes. *J Biol Chem* 271: 390–394, 1996.
6. Biswas M and Chan JY. Role of Nrf1 in antioxidant response element-mediated gene expression and beyond. *Toxicol Appl Pharmacol* 244: 16–20, 2010.
7. Buettner C. Is hyperinsulinemia required to develop overeating-induced obesity? *Cell Metab* 16: 691–692, 2012.
8. Chan JY, Kwong M, Lu R, Chang J, Wang B, Yen TS, and Kan YW. Targeted disruption of the ubiquitous CNC-bZIP transcription factor, Nrf-1, results in anemia and embryonic lethality in mice. *EMBO J* 17: 1779–1787, 1998.
9. Corkey BE. Banting lecture 2011: hyperinsulinemia: cause or consequence? *Diabetes* 61: 4–13, 2012.
10. Costes S, Huang CJ, Gurlo T, Daval M, Matveyenko AV, Rizza RA, Butler AE, and Butler PC. Beta-cell dysfunctional ERAD/ubiquitin/proteasome system in type 2 diabetes mediated by islet amyloid polypeptide-induced UCH-L1 deficiency. *Diabetes* 60: 227–238, 2011.
11. Donath MY, Boni-Schnetzler M, Ellingsgaard H, and Ehses JA. Islet inflammation impairs the pancreatic beta-cell in type 2 diabetes. *Physiology (Bethesda)* 24: 325–331, 2009.
12. Donath MY, Ehses JA, Maedler K, Schumann DM, Ellingsgaard H, Eppler E, and Reinecke M. Mechanisms of {beta}-cell death in type 2 diabetes. *Diabetes* 54 Suppl 2: S108–S113, 2005.
13. Fu J, Woods CG, Yehuda-Shnaidman E, Zhang Q, Wong V, Collins S, Sun G, Andersen ME, and Pi J. Low-level arsenic impairs glucose-stimulated insulin secretion in pancreatic beta cells: involvement of cellular adaptive response to oxidative stress. *Environ Health Perspect* 118: 864–870, 2011.
14. Hartley T, Brumell J, and Volchuk A. Emerging roles for the ubiquitin-proteasome system and autophagy in pancreatic beta-cells. *Am J Physiol Endocrinol Metab* 296: E1–E10, 2009.
15. Henquin JC. Pathways in beta-cell stimulus-secretion coupling as targets for therapeutic insulin secretagogues. *Diabetes* 53 Suppl 3: S48–S58, 2004.
16. Henquin JC. The dual control of insulin secretion by glucose involves triggering and amplifying pathways in beta-cells. *Diabetes Res Clin Pract* 93 Suppl 1: S27–S31, 2011.
17. Henquin JC. Do Pancreatic beta cells ''Taste'' nutrients to secrete insulin? *Sci Signal* 5: pe36, 2012.
18. Henquin JC, Ravier MA, Nenquin M, Jonas JC, and Gilon P. Hierarchy of the beta-cell signals controlling insulin secretion. *Eur J Clin Invest* 33: 742–750, 2003.
19. Hirotsu Y, Hataya N, Katsuoka F, and Yamamoto M. NF-E2-related factor 1 (Nrf1) serves as a novel regulator of hepatic lipid metabolism through regulation of the Lipin1 and PGC-1beta genes. *Mol Cell Biol* 32: 2760–2770, 2012.
20. Kim J, Xing W, Wergedal J, Chan JY, and Mohan S. Targeted disruption of nuclear factor erythroid-derived 2-like 1 in osteoblasts reduces bone size and bone formation in mice. *Physiol Genomics* 40: 100–110, 2010.
21. Kobayashi A, Tsukide T, Miyasaka T, Morita T, Mizoroki T, Saito Y, Ihara Y, Takashima A, Noguchi N, Fukamizu A, Hirotsu Y, Ohtsuji M, Katsuoka F, and Yamamoto M. Central nervous system-specific deletion of transcription factor Nrf1 causes progressive motor neuronal dysfunction. *Genes Cells* 16: 692–703, 2011.
22. Kong D, Tong Q, Ye C, Koda S, Fuller PM, Krashes MJ, Vong L, Ray RS, Olson DP, and Lowell BB. GABAergic RIP-Cre neurons in the arcuate nucleus selectively regulate energy expenditure. *Cell* 151: 645–657, 2012.
23. Kwong EK, Kim KM, Penalosa PJ, and Chan JY. Characterization of Nrf1b, a novel isoform of the nuclear factor-erythroid-2 related transcription factor-1 that activates antioxidant response element-regulated genes. *PLoS One* 7: e48404, 2012.
24. Kwong M, Kan YW, and Chan JY. The CNC basic leucine zipper factor, Nrf1, is essential for cell survival in response to oxidative stress-inducing agents. Role for Nrf1 in gamma-gcs(l) and gss expression in mouse fibroblasts. *J Biol Chem* 274: 37491–37498, 1999.
25. Lee CS, Lee C, Hu T, Nguyen JM, Zhang J, Martin MV, Vawter MP, Huang EJ, and Chan JY. Loss of nuclear factor E2-related factor 1 in the brain leads to dysregulation of proteasome gene expression and neurodegeneration. *Proc Natl Acad Sci U S A* 108: 8408–8413, 2011.
26. Lee JY, Ristow M, Lin X, White MF, Magnuson MA, and Hennighausen L. RIP-Cre revisited, evidence for impairments of pancreatic beta-cell function. *J Biol Chem* 281: 2649–2653, 2006.
27. Levine AJ and Puzio-Kuter AM. The control of the metabolic switch in cancers by oncogenes and tumor suppressor genes. *Science* 330: 1340–1344, 2010.
28. Lowell BB and Shulman GI. Mitochondrial dysfunction and type 2 diabetes. *Science* 307: 384–387, 2005.
29. Magnuson MA and Osipovich AB. Pancreas-specific Cre driver lines and considerations for their prudent use. *Cell Metab* 18: 9–20, 2013.
30. Maiztegui B, Borelli MI, Massa ML, Del Zotto H, and Gagliardino JJ. Enhanced expression of hexokinase I in

pancreatic islets induced by sucrose administration. *J Endocrinol* 189: 311–317, 2006.
31. Malmgren S, Nicholls DG, Taneera J, Bacos K, Koeck T, Tamaddon A, Wibom R, Groop L, Ling C, Mulder H, and Sharoyko VV. Tight coupling between glucose and mitochondrial metabolism in clonal beta-cells is required for robust insulin secretion. *J Biol Chem* 284: 32395–32404, 2009.
32. Mehran AE, Templeman NM, Brigidi GS, Lim GE, Chu KY, Hu X, Botezelli JD, Asadi A, Hoffman BG, Kieffer TJ, Bamji SX, Clee SM, and Johnson JD. Hyperinsulinemia drives diet-induced obesity independently of brain insulin production. *Cell Metab* 16: 723–737, 2012.
33. Ohtsuji M, Katsuoka F, Kobayashi A, Aburatani H, Hayes JD, and Yamamoto M. Nrf1 and Nrf2 play distinct roles in activation of antioxidant response element-dependent genes. *J Biol Chem* 283: 33554–33562, 2008.
34. Pi J, Bai Y, Daniel KW, Liu D, Lyght O, Edelstein D, Brownlee M, Corkey BE, and Collins S. Persistent oxidative stress due to absence of uncoupling protein 2 associated with impaired pancreatic beta-cell function. *Endocrinology* 150: 3040–3048, 2009.
35. Pi J, Bai Y, Zhang Q, Wong V, Floering LM, Daniel K, Reece JM, Deeney JT, Andersen ME, Corkey BE, and Collins S. Reactive oxygen species as a signal in glucose-stimulated insulin secretion. *Diabetes* 56: 1783–1791, 2007.
36. Prentki M and Nolan CJ. Islet beta cell failure in type 2 diabetes. *J Clin Invest* 116: 1802–1812, 2006.
37. Radhakrishnan SK, Lee CS, Young P, Beskow A, Chan JY, and Deshaies RJ. Transcription factor Nrf1 mediates the proteasome recovery pathway after proteasome inhibition in mammalian cells. *Mol Cell* 38: 17–28, 2010.
38. Robertson RP. Oxidative stress and impaired insulin secretion in type 2 diabetes. *Curr Opin Pharmacol* 6: 615–619, 2006.
39. Schuit F, Van Lommel L, Granvik M, Goyvaerts L, de Faudeur G, Schraenen A, and Lemaire K. Beta-cell-specific gene repression: a mechanism to protect against inappropriate or maladjusted insulin secretion? *Diabetes* 61: 969–975, 2012.
40. Steffen J, Seeger M, Koch A, and Kruger E. Proteasomal degradation is transcriptionally controlled by TCF11 *via* an ERAD-dependent feedback loop. *Mol Cell* 40: 147–158, 2010.
41. Stumvoll M, Goldstein BJ, and van Haeften TW. Type 2 diabetes: principles of pathogenesis and therapy. *Lancet* 365: 1333–1346, 2005.
42. Wang W, Kwok AM, and Chan JY. The p65 isoform of Nrf1 is a dominant negative inhibitor of ARE-mediated transcription. *J Biol Chem* 282: 24670–24678, 2007.
43. Wicksteed B, Brissova M, Yan W, Opland DM, Plank JL, Reinert RB, Dickson LM, Tamarina NA, Philipson LH, Shostak A, Bernal-Mizrachi E, Elghazi L, Roe MW, Labosky PA, Myers MG, Jr., Gannon M, Powers AC, and Dempsey PJ. Conditional gene targeting in mouse pancreatic ss-cells: analysis of ectopic Cre transgene expression in the brain. *Diabetes* 59: 3090–3098, 2010.
44. Xu Z, Chen L, Leung L, Yen TS, Lee C, and Chan JY. Liver-specific inactivation of the Nrf1 gene in adult mouse leads to nonalcoholic steatohepatitis and hepatic neoplasia. *Proc Natl Acad Sci U S A* 102: 4120–4125, 2005.
45. Xue P, Hou Y, Chen Y, Yang B, Fu J, Zheng H, Yarborough K, Woods CG, Liu D, Yamamoto M, Zhang Q, Andersen ME, and Pi J. Adipose deficiency of Nrf2 in ob/ob mice results in severe metabolic syndrome. *Diabetes* 62: 845–854, 2013.
46. Xue P, Hou Y, Zhang Q, Woods CG, Yarborough K, Liu H, Sun G, Andersen ME, and Pi J. Prolonged inorganic arsenite exposure suppresses insulin-stimulated AKT S473 phosphorylation and glucose uptake in 3T3-L1 adipocytes: Involvement of the adaptive antioxidant response. *Biochem Biophys Res Commun* 407: 360–365, 2011.
47. Zhang Y and Hayes JD. The membrane-topogenic vectorial behaviour of Nrf1 controls its post-translational modification and transactivation activity. *Sci Rep* 3: 2006, 2013.
48. Zhang Y, Lucocq JM, Yamamoto M, and Hayes JD. The NHB1 (N-terminal homology box 1) sequence in transcription factor Nrf1 is required to anchor it to the endoplasmic reticulum and also to enable its asparagine-glycosylation. *Biochem J* 408: 161–172, 2007.
49. Zhao R, Hou Y, Xue P, Woods CG, Fu J, Feng B, Guan D, Sun G, Chan JY, Waalkes MP, Andersen ME, and Pi J. Long isoforms of NRF1 contribute to arsenic-induced antioxidant response in human keratinocytes. *Environ Health Perspect* 119: 56–62, 2011.
50. Zhao R, Hou Y, Zhang Q, Woods CG, Xue P, Fu J, Yarborough K, Guan D, Andersen ME, and Pi J. Cross-regulations among NRFs and KEAP1 and effects of their silencing on arsenic-induced antioxidant response and cytotoxicity in human keratinocytes. *Environ Health Perspect* 120: 583–589, 2012.

Address correspondence to:
Dr. Jingbo Pi
School of Public Health
China Medical University
77 Puhe Road
Shenyang North New Area
Shenyang 110013
China

E-mail: jingbopi@163.com
jpi@mail.cmu.edu.cn

Dr. Weiping Teng
The First Affiliated Hospital
China Medical University
No. 155 Nanjing North St.
Heping, Shenyang 110001
China

E-mail: twp@vip.163.com

Date of first submission to ARS Central, June 11, 2014; date of acceptance, January 1, 2015.

Abbreviations Used

aa = amino acids
AMPKα = AMP-activated protein kinase α
ATPase = gamma subunit of ATP synthase F1 complex
BSA = bovine serum albumin
CYC = cytochrome c
2-DG = 2-deoxy-D-glucose
DMEM = Dulbecco's modified Eagle's medium
ECAR = extracellular acidification rate
ER = endoplasmic reticulum
FBS = fetal bovine serum

Abbreviations Used (Cont.)

FCCP = trifluorocarbonylcyanide phenylhydrazone
GAPDH = glyceraldehyde 3-phosphate dehydrogenase
GCK = glucokinase
GLUT2 = glucose transporter 2
GSH = reduced glutathione
GSIS = glucose-stimulated insulin secretion
GSSG = oxidized glutathione
HG = high glucose
HIF1α = hypoxia-induced factor 1α
HK1 = hexokinase 1
HOMA-IR = homeostatic model assessment for insulin resistance
IPGTT = intraperitoneal glucose tolerance test
KI = knock-in
KO = knockout
LDH1 = lactate dehydrogenase 1
LG = low glucose
MTCO1 = complex I
MTCO2 = complex II
Nrf1 = nuclear factor-erythroid 2-related factor 1
MW = molecular weight
Nrf1(b)-KO = β-cell-specific *Nrf1*-knockout
Nrf1-KD = Nrf1-knockdown
OCR = oxygen consumption rate
PBS = phosphate-buffered saline
PGC1α = peroxisome proliferator-activated receptor gamma coactivator 1α
qPCR = quantitative real-time PCR
ROS = reactive oxygen species
RT-PCR = reverse transcription-polymerase chain reaction
RT-qPCR = reverse transcription-quantitative polymerase chain reaction
T2D = type 2 diabetes
TFs = transcription factors
UPS = ubiquitin-proteasome system
WT = wild-type